Journal of Colloid and Interface Science 445 (2015) 285–293

Contents lists available at ScienceDirect

Journal of Colloid and Interface Science

www.elsevier.com/locate/jcis

Self-assembly of myristic acid in the presence of choline hydroxide: Effect of molar ratio and temperature

Audrey Arnould [a], Adrian A. Perez [b], Cédric Gaillard [a], Jean-Paul Douliez [c], Fabrice Cousin [d], Liliana G. Santiago [b], Thomas Zemb [e], Marc Anton [a], Anne-Laure Fameau [a,*]

[a] INRA, UR1268 Biopolymères Interactions Assemblages, F-44316 Nantes, France
[b] Grupo de Biocoloides, Instituto de Tecnología de Alimentos, Universidad Nacional del Litoral, 1 de Mayo 3250 (3000), Santa Fe, Argentina
[c] Biologie et Pathologie du Fruit, UMR 1332, INRA, Centre de Bordeaux, 33883 Villenave d'Ornon, France
[d] Laboratoire Léon Brillouin, CEA-CNRS, CEA Saclay, 91191 Gif sur Yvette Cedex, France
[e] Institut de Chimie Séparative de Marcoule (ICSM), UMR 5257, CEA-CNRS-Université Montpellier 2-ENSCM, F-30207 Bagnols-sur-Cèze Cedex, France

GRAPHICAL ABSTRACT

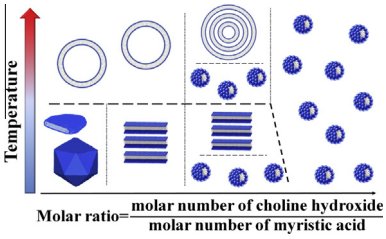

ARTICLE INFO

Article history:
Received 19 December 2014
Accepted 6 January 2015
Available online 14 January 2015

Keywords:
Fatty acid
Counter-ion
Molar ratio
Self-assembly
Catanionic

ABSTRACT

Salt-free catanionic systems based on fatty acids exhibit a broad polymorphism by simply tuning the molar ratio between the two components. For fatty acid combined with organic amino counter-ions, very few data are available on the phase behavior obtained as a function of the molar ratio between the counter-ion and the fatty acid. We investigated the choline hydroxide/myristic acid system by varying the molar ratio, $R = n_{\text{choline hydroxide}}/n_{\text{myristic acid}}$, and the temperature. Myristic acid ionization state was determined by coupling pH, conductivity and infra-red spectroscopy measurements. Self-assemblies were characterized by small angle neutron scattering and microscopy experiments. Self-assembly thermal behavior was investigated by differential scanning calorimetry, wide angle X-ray scattering and nuclear magnetic resonance. For $R < 1$, ionized and protonated myristic acid molecules coexisted leading to the formation of facetted self-assemblies and lamellar phases. The melting process between the gel and the fluid state of these bilayers induced a structural change from facetted or lamellar objects to spherical vesicles. For $R > 1$, myristic acid molecules were ionized and formed spherical micelles. Our study highlights that both R and temperature are two key parameters to finely control the self-assembly structure formed by myristic acid in the presence of choline hydroxide.

1. Introduction

Fatty acids are a simple class of anionic biocompatible surfactants when they are ionized [1]. They are available in large amount in nature and can be extracted from plant oils or from waste by-products such as tomato peels [2,3]. These biomolecules can be used for various applications in cosmetic, washing, environmental clean-up, material recovery processes, encapsulation and drug delivery [4]. The most well-known application is the so-called fatty acid soaps, i.e. sodium or potassium salts of fatty acids, which are used for hundreds of years as household cleaning products [1,3].

* Corresponding author.
E-mail address: anne-laure.fameau@nantes.inra.fr (A.-L. Fameau).

http://dx.doi.org/10.1016/j.jcis.2015.01.008
0021-9797/

The main constraint with fatty acids as surfactants is their poor solubility in aqueous solution at room temperature [5]. The Krafft point of fatty acids increases rapidly with the alkyl chain length corresponding to a decrease in solubility [6,7], which hampers the use of long chain fatty acids for many applications, despite of their promising interfacial and foaming properties [4,8–10].

To face this drawback, various methods have been considered to enhance the solubility of fatty acids in water [11]. In 1973, Gebicki and Hicks were the first to report the formation of fatty acid vesicles in aqueous solution from oleic acid and sodium oleate interacting by hydrogen bonding [12]. In the last decade, other physical-chemistry approaches have been designed such as the formation of catanionic systems by adding cationic surfactants under hydroxide form leading to salt-free systems [11,13]. One of the most important parameters in these catanionic systems is the molar ratio between both species [11]. For example, by mixing myristic acid and cetyltrimethylammonium hydroxide (CTAOH) at different molar ratios, various self-assemblies have been obtained such as micelles, vesicles, nanodiscs or icosahedra [11,14–16]. Along the same lines, many results have been obtained for fatty acid systems in the presence of trimethyltetradecylammonium hydroxide (TTAOH) [17]. For example, for lauric acid with TTAOH at 25 °C, micelles are obtained in excess of TTAOH, whereas vesicles are formed at equimolarity. These examples clearly demonstrate that the molar ratio has a strong influence on the self-assembled morphology and governs other important parameters such as the ionization state of fatty acids, the hydrogen bonds, the Krafft point and the melting transition [11,17,18].

Another way to disperse fatty acids in aqueous solution consists in using bulky soluble organic amino counter-ions which interacts by ion-pairing with fatty acids and increase the fatty acid solubility [11,19]. As for catanionic systems, dispersions of fatty acids in the presence of amino counter-ions lead to various self-assemblies such as micelles, vesicles, tubes, and cones [11,19]. Recently, amine components from biological origin such as choline, lysine or guanidine have been used as counter-ion to disperse fatty acids [2,11,20,21]. Choline, a quaternary ammonium ion considered as an essential nutrient, is a biocompatible molecule and is safe for environment because of its natural decomposition [22,23]. This molecule, weakly hydrated, acts as a chaotrope and improves the fatty acid dispersion. In diluted systems (<5 wt%), fatty acids with choline can form spherical or worm-like micelles depending on the alkyl chain length [24]. Various liquid crystalline phases have also been obtained at higher concentration [25–27]. An interesting point of these systems is that by adding an excess of choline hydroxide, it is possible to drastically lower the Krafft point in diluted systems. At equimolar ratio between choline and stearic acid, the Krafft point is around 40 °C whereas for an excess of choline hydroxide, the Krafft point decreases down to 15 °C [25]. Thus, the molar ratio between the choline hydroxide and the fatty acid seems to be a crucial parameter in these systems.

To our knowledge, few data are available on the effect of the molar ratio on the phase behavior in a fatty acid system in the presence of organic quaternary ammonium counter-ion under hydroxide form conversely to catanionic systems [11]. The aim of this study is to investigate such a system as a function of both the molar ratio and the temperature. As a model system, we used myristic acid and choline under its hydroxide form, as quaternary ammonium counter-ion (Fig. 1). The molar ratio R is given by $R = n_{\text{choline hydroxide}}/n_{\text{myristic acid}}$, with n the molar concentration. The fatty acid concentration was fixed at 10 mg/mL (1 wt%) to focus on the diluted regime. Our strategy was to establish the link between the polymorphism, the ionization state of fatty acids and the melting transition as a function of both R and temperature by combining experiments at different length scales. By coupling conductivity, pH measurements and Fourier Transform Infra-red spectroscopy (FT-IR), we investigated the ionization state of fatty acids as a function of R. We performed Small Angle Neutron Scattering (SANS) measurements and microscopy observations to characterize the morphology of the self-assemblies. To determine the melting transition of the alkyl chains, Differential Scanning Calorimetry (DSC), solid-state Nuclear Magnetic Resonance (NMR) and Wide-Angle X-ray Scattering (WAXS) were used.

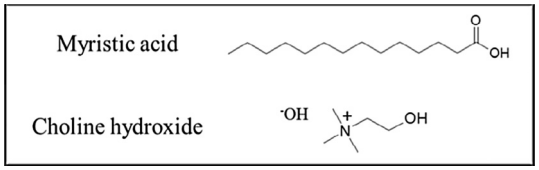

Fig. 1. Molecular structure of the myristic acid and choline hydroxide used in this study.

2. Materials and method

2.1. Sample preparation

Myristic acid (purity > 99%) and choline hydroxide (46 wt% in H_2O) were purchased from Sigma Aldrich and were used as received. Myristic acid was weighted exactly in a tube and ultrapure water was added so that the concentration was 10 mg/mL (1% weight in water). Next, the desired volume of a 1 mol L^{-1} choline hydroxide solution prepared in ultrapure water was incorporated to reach the desired molar ratio defined as $R = n_{\text{choline hydroxide}}/n_{\text{myristic acid}}$ with n the molar concentration in mol L^{-1}. The mixture was heated at 75 °C during 5 min and frozen several times until the fatty acid powder was fully dispersed. Samples were further stored at −18 °C and prior to be used, they were heated at 75 °C during 5 min and cooled to room temperature.

2.2. Phase behavior

Binary phase diagram was established by visual inspection with the help of crossed polarizers. The temperature was controlled by a water bath or an oven and was varied from 10 °C to 50 °C. All the samples were kept at least four days at a given temperature to be close to equilibrium before observing the phase behavior.

2.3. pH and conductivity measurements

The pH measurements were performed on a TIM900 Titration Manager (Radiometer) at 20 °C. The conductivity measurements were performed on a CDM230 conductivity meter (Radiometer). Samples were stirred during the measurements. The pH and conductivity values for each sample are the average of three measurements.

2.4. Fourier transform infrared spectra (FT-IR)

FT-IR spectra were recorded on a Nicolet Magna IR 550 Serie II (nitrogen cooled mercury–cadmium–telluride detector, KBr beamsplitter) with a resolution of 2 cm^{-1} at room temperature (24 °C). Samples were spread on the selenium chloride crystal. The instrument was continuously purged with dry air. To improve the signal to noise ratio, 200 scans were averaged for each sample. The baseline subtraction and offset corrections were done by using the Galactic GRAM/AI 7.0 software.

2.5. Small and very small angle neutron scattering (SANS and VSANS)

SANS and VSANS experiments were performed at Laboratoire Léon Brillouin (Saclay, France). Samples were prepared with deuterated water and were held in flat quartz cells with a 2 mm optical path length. The PACE spectrometer was used for the SANS experiments. Three configurations were chosen to get a Q-range lying between $5 \cdot 10^{-3}$ and $3 \cdot 10^{-1}$ Å^{-1} (respectively 5 Å at 1 m, 5 Å at 4.7 m and 13 Å at 4.7 m) with a significant overlap between the three configurations. The temperature was controlled by a circulating fluid to within ±0.2 °C. The neutron wavelength was set to the desired value with a mechanical velocity selector ($\Delta\lambda/\lambda \approx 0.1$). The azimuthally averaged spectra were corrected for solvent, empty cell, as well as background noise, and were normalized to the incoherent H_2O signal by using PASINET software package provided at the beamline [28]. The VSANS experiments were performed at spectrometer TPA [29]. The sample to detector distance was 6.187 m and the neutron wavelength 6 Å to reach low scattering vectors Q lying between $6 \cdot 10^{-4}$ and $5 \cdot 10^{-3}$ Å^{-1}. As for SANS experiments, temperature was controlled by a circulating fluid to within ±0.5 °C. The empty quartz cell and electronic background were subtracted by using the PAsiNET software. All the form factors used to fit the SANS data are described in Supporting Information.

2.6. Transmission electronic microscopy (TEM) and cryo-TEM observations

Samples for cryo-TEM observation were prepared using a cryo-plunge cryo-fixation device (Gatan, USA) in which a drop of the aqueous suspension was deposited on to glow-discharged holey-type carbon-coated grids (Ted Pella Inc., USA). The TEM grid was then prepared by blotting the drop containing the self-assemblies to a thin liquid layer remained across the holes in the support carbon film. The liquid film was vitrified by rapidly plunging the grid into liquid ethane cooled by liquid nitrogen. The vitrified samples were mounted in a Gatan 910 specimen holder that was inserted in the microscope using a CT-3500-cryotransfer system and cooled with liquid nitrogen. Cryo-TEM images were then obtained from samples preserved in vitreous ice and suspended across a hole in the supporting carbon substrate using a JEM 1230 'Cryo' microscope (Jeol, Japan) operated at 80 kV and equipped with a LaB6 filament. For the conventional TEM experiments, a drop of each sample was placed on a carbon-coated TEM copper grid and negatively stained with uranyl acetate. The grid was then air-dried before observation.

2.7. Phase contrast microscopy observations

Phase contrast microcopy observations were performed at different temperatures (15–40 °C) at 40× magnification using an optical microscope in the phase contrast mode (Nikon Eclipse E-400) equipped with a STC-CM202 USB color camera (Sentech) allowing digital images (1600 × 1200 pixels) to be collected. A drop of the aqueous dispersion (about 20 μL) was deposited onto a coverslide (24 × 60 mm, Menzel Gläser) and covered by another coverslide (18 × 18 mm, Menzel Gläser). The coverslides were cleaned with ethanol before using.

2.8. Differential Scanning Calorimetry (DSC) measurements

The phase transition temperature was measured on a microcalorimeter Micro-DSC 7 (Setaram, France). Two stainless steel cells were used, one containing ca. 0.75 g of sample and the other, filled with the same amount of water used as reference. The heating and cooling ramp was from 5 °C to 75 °C at a rate of 0.5 °C/min. The data analysis was performed with Calisto Processing and Origin Pro 8 software.

2.9. Solid-state nuclear magnetic resonance (NMR)

Deuterium solid-state NMR measurements were performed at several temperatures from 10 °C to 35 °C on a 400 MHz Bruker spectrometer (Wissembourg, France) operating at 61 MHz for deuterium using a static double channel probe. Samples were prepared using perdeuterated myristic acid (Eurisotop, France) at a concentration of 2 wt%, dispersed in de-deuterated water (Eurisotop, France) and the desired volume of a 1 mol L^{-1} choline hydroxide solution (also prepared in de-deuterated water) was further added. Samples were prepared as described previously. The sample coil of the probe was adapted to load a 7 mm outer diameter sample tube containing about 400 μL of the fatty acid dispersion. A Hahn quadrupolar echo sequence was used with an inter pulse delay of 40 μs. A total of 4 k points in 1 k accumulations (every 2 s) were done with a 90° pulse and a spectral width of 6 μs and 500 kHz, respectively. Free induction decay signals were zero-filled to 8 k points prior Fournier transform after a broad line exponential multiplication of 100 Hz. The general theory to determine the fluidity of lipid bilayer systems by deuterium spectroscopy can be found in the literature and is summarized in the Supporting Information [30].

2.10. Wide angle X-ray scattering (WAXS)

Diffraction diagrams were monitored by recording X-ray diffraction diagrams every 30 min on a Bruker D8 Discover diffractometer. Cu Ka_1 radiation (Cu Ka_1 = 1.5405 Å), produced in a sealed tube at 40 kV and 40 mA was selected and parallelized using a Gobël mirror parallel optics system and collimated to produce a 0.5 cm beam diameter. Samples were prepared using the previous procedure with a myristic acid concentration at 2% put in thin capillaries of 1.5 mm of diameter which were then flame-sealed immediately. The temperature was changed from 15 °C to 35 °C and controlled by a HFS 91-CAP platine (Linkam).

3. Results

3.1. Phase behavior in the choline hydroxide/myristic acid system

We studied the mixture between choline hydroxide and myristic acid which the chemical structures are shown in Fig. 1. The myristic acid concentration was fixed at 10 mg mL^{-1} to focus on the diluted regime. The molar ratio between choline hydroxide and myristic acid was defined as $R = n_{\text{choline hydroxide}}/n_{\text{myristic acid}}$. All the samples were equilibrated four days at a given temperature before observing the phase behavior. For $R < 0.4$, myristic acid crystals were observed indicating that the amount of choline hydroxide was not sufficient to disperse the myristic acid (Fig. SI1). Then, the molar ratio R was varied from 0.4 to 2 and various phases were observed as a function of the temperature. The phase diagram obtained as a function of both R and temperature is illustrated Fig. 2a. Pictures of samples within each phase regions are shown in Fig. 2b. Additional pictures can be found in the Supporting Information (Fig. SI2).

In region I, corresponding to $0.4 \leqslant R < 0.45$ at all temperatures and $0.45 \leqslant R \leqslant 0.55$ at $T > 30$ °C, a homogenous turbid phase without birefringence was observed between crossed polarizers (Fig. 2b). At low temperature ($T < 30$ °C) and for $0.45 \leqslant R \leqslant 0.55$, a homogenous turbid phase with birefringence was observed between crossed polarizers, which corresponds to region II (Fig. 2b). This birefringence suggests the formation of lamellar structures in solution. For R lying in the range 0.55–0.8, a slow

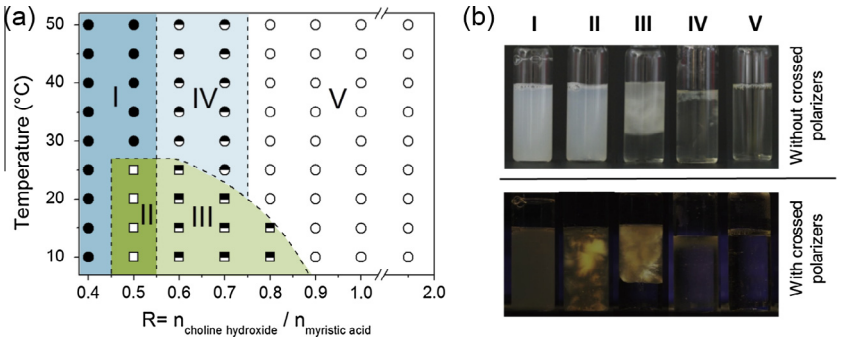

Fig. 2. (a) Phase diagram of the choline hydroxide/myristic acid system as a function of temperature and molar ratio *R*. The myristic acid concentration was 10 mg/mL. (b) Different phases have been observed with and without crossed polarizers. I: turbid without birefringence (dark circles), II: turbid with birefringence (open squares), III: phase separation with an upper turbid phase with birefringence and a lower limpid phase (back and white squares), IV: phase separation with an upper turbid phase without birefringence and a lower limpid phase (black and white circle), V: limpid without birefringence (open circle). The pictures for Regions I, II, III, IV and V correspond to $R = 0.4$ at 15 °C, $R = 0.5$ at 15 °C, $R = 0.7$ at 15 °C, $R = 0.7$ at 35 °C and $R = 1$ at 15 °C, respectively.

macroscopic phase separation occurred progressively with time within few hours for all temperatures leading to a two-phase region. At low temperature ($T < 30$ °C), the upper phase was turbid with birefringence and the lower phase was limpid (Fig. 2b). This corresponds to the region III. At higher temperature ($T > 30$ °C), the birefringent texture was no longer observed in the upper turbid phase, and the lower phase remained limpid which corresponds to region IV (Fig. 2b). At higher molar ratio ($R \geqslant 0.9$) for all temperatures, a limpid phase was observed (region V).

3.2. Ionization state of fatty acids as a function of R

The ionization state of fatty acids is a crucial parameter governing the formation of hydrogen bonding and the electrostatic interactions at the origin of various self-assemblies [11,31]. In order to determine the ionization state of the myristic acid in the presence of choline hydroxide as a function of *R*, we performed pH and conductivity measurements coupled with Fourier Transform Infra-red (FT-IR) spectroscopy experiments.

The pH and conductivity were measured as a function of *R*, half an hour after equilibration at room temperature prior to phase separation occurs (Fig. 3). At low molar ratio ($0.4 \leqslant R < 1$), pH was almost constant around 9.2 +/−0.2. From $R = 1.0$ to $R = 1.2$, pH increased sharply to reach a value of 12. For $R > 1.2$, the pH did not evolve anymore and remained constant around 12. The pH jump around equimolarity reveals a titration of the myristic acid by the hydroxide ion. The conductivity was very low for $0.4 \leqslant R < 1$ and increased slightly from 0.3 to 1.5 mS cm^{-1}. From equimolarity ($R = 1$), the conductivity increased drastically with *R*. The corresponding FT-IR spectra obtained at room temperature are represented in Fig. 4a. We focused on two peaks at 1565 cm^{-1} and 1700 cm^{-1}, which correspond to the characteristic bands of COO^- and COOH, respectively.

For $R < 1$, both peaks were observed, which confirms the coexistence of ionized and protonated form of myristic acid in this pH range ($9.0 < pH < 9.4$). The hydroxide ions react with the carboxylic acid of myristic acid to form water and ionized myristic acid. Both hydroxide ion and choline cation, which interact with the carboxylic or carboxylate groups, do not contribute to the conductivity leading to low conductivity. Upon increasing *R*, we observed that the intensity of the peak at 1700 cm^{-1} decreased whereas the intensity of the peak at 1565 cm^{-1} increased. An increase of *R* led to a progressive decrease of the quantity of protonated fatty acid in solution. It is well known that by increasing the pH, fatty acids become progressively ionized [31]. We also observed that the wavenumbers at which the peaks appear were slightly shifted from 1565 cm^{-1} to 1575 cm^{-1} for the characteristic band of COO^-

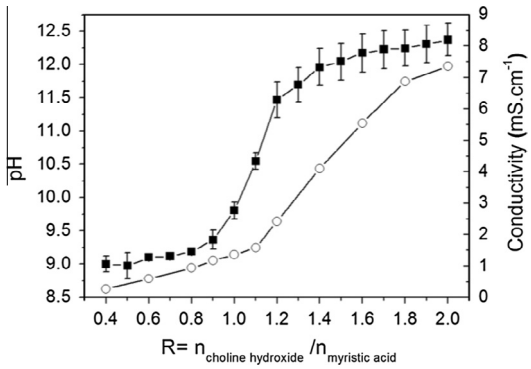

Fig. 3. Evolution of pH (■) and conductivity (○) as a function of the molar ratio *R*. Measurements was performed at 20 °C under stirring.

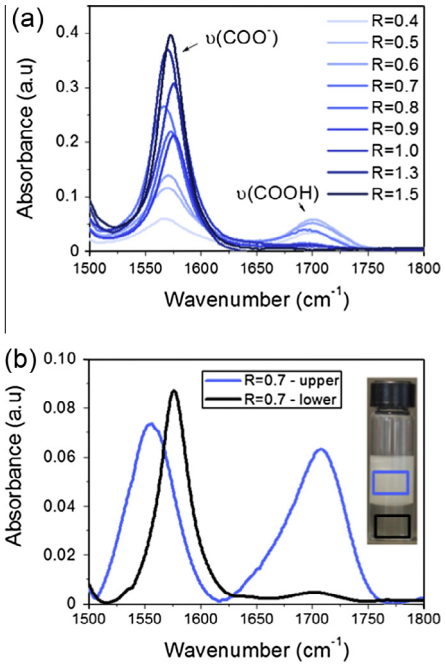

Fig. 4. (a) FT-IR spectra for the choline hydroxide/myristic acid system as a function of the molar ratio *R* before phase separation at 24 °C. (b) FT-IR spectra after phase separation occurred for the two separated phases of the region IV ($R = 0.7$). The upper phase was turbid with birefringence and the lower phase was limpid.

and from 1700 cm^{-1} to 1693 cm^{-1} for the characteristic band of COOH, depending on the value of *R*. In the literature, this shift is attributed to the formation of hydrogen bonds [32].

For $R > 1$, only the peak at 1565 cm^{-1} was observed which is consistent with fatty acids fully ionized, what is expected at such a high pH value (pH around 12). Thus, hydroxide ions cannot react anymore with the carboxylic acid of myristic acid. The addition of hydroxide ions in excess upon increasing *R* in the aqueous solution contributes then directly to the conductivity of the solution, explaining the large increase of such conductivity. In summary, for $R < 1$, the turbid samples in regions I, II and III were composed of both ionized and protonated myristic acid molecules. In region V, the limpid solution was composed only by ionized myristic acid. Thus, by tuning *R*, which in turn changes the pH of the solution, the ionization state of myristic acid can be modified.

To get information at the molecular scale on the ionization state for samples in Region III, where phase separation occurred with time, FT-IR measurements for each phase after equilibration at room temperature were performed. The FT-IR spectra for $R = 0.7$ are shown in Fig. 4b and for $R = 0.6$ in Fig. SI3. For the upper turbid phase, both peaks at around 1565 cm^{-1} and 1700 cm^{-1} were observed, whereas only the peak at 1575 cm^{-1} was observed for the lower limpid phase. The upper turbid phase was then composed of both the ionized and the protonated forms of the fatty acid, whereas the lower limpid phase contained only ionized fatty acid molecules. In region III, a molecular segregation occurred and the protonated fatty acids were only present in the upper phase.

3.3. Self-assemblies characterized by Small and Very Small Angle Neutron Scattering (SANS and VSANS) and microscopy experiments

In order to characterize the self-assemblies in solution in the various regions shown in Fig. 2a, SANS experiments were performed for various *R* and temperatures. Fig. 5 displays the scattering profiles for $R = 0.4$ (a), $R = 0.5$ (b), $R = 0.6$ (c) and $R = 1.0$ (d) with the corresponding microscopy images in the different regions of the phase diagram.

In region I, for $R = 0.4$, the presence of large bilayer structures in solution was evidenced from the Q^{-2} decay of the scattered intensity over more than two decades at 15 °C (Fig. SI4a) and at 25 °C (Fig. 5a). At large-Q, in the Porod regime, the oscillation of the bilayer form factor was observed. The bilayer thickness was estimated to be around 36 Å at 25 °C from the modeling of the scattered intensity, which corresponds to almost twice the chain length of myristic acid in the extended conformation confirming the presence of bilayer structures in solution (Fig. SI5a). By coupling Cryo-TEM and phase contrast microscopy experiments, we observed facetted self-assemblies: micron-size facetted discs (Fig. 5a, left image) and large facetted vesicles displaying polydispersity in shape and size (Fig. SI6a and b). For $R = 0.4$, at 35 °C, the SANS spectrum was similar to the one obtained at 25 °C. The Q^{-2} decay was still observed and only the oscillation of the bilayer form factor was shifted to higher Q meaning that the bilayer thickness decreased and was around 30 Å at 35 °C (Fig. SI5a). In this region, only spherical polydispersed large vesicles were observed by phase contrast microscopy (Fig. 5a, right image and SI6c). In region I, the solution was turbid without birefringence due to the presence of facetted objects (discs and vesicles) or spherical vesicles as a function of the temperature. Then, we can refine the phase diagram obtained by visual observations and we divided the region I into region I.A (facetted objects) and region I.B (spherical vesicles) in the Scheme 1.

In region II, for $R = 0.5$ and $T < 30$ °C, the scattering curve still exhibited a Q^{-2} decay indicating that large bilayer structures were present in solution (Fig. 5b and SI4b). Three peaks were present in the intermediate-Q region, whose position can be readily identified in the ratio 1:2:3 (Q_0, 2 Q_0, 3 Q_0). The presence of a strong correlation peak followed by its harmonics indicated the presence of stacked lamellar phases in solution consistent with the turbidity and the birefringence observed for the samples in this region. The lamellar spacing, corresponding to the repeat distance to one lipid bilayer and one water layer in the stack, was estimated from the first peak position at around 370 Å ($2\pi/Q_0$). At large-Q, the bilayer thickness was determined at around 31 Å at 25 °C from the oscillation of the form factor (Fig. SI5b). The presence of lamellar phases in solution was further confirmed by TEM and phase contrast microscopy experiments as shown in Fig. 5b (left image) and Fig. SI6d–e. By increasing the temperature up to 35 °C at $R = 0.5$, the lamellar structure disappeared and the typical scattering feature of a bilayer was recovered (Fig. 5b), as already observed in region I.B of the phase diagram at $R = 0.4$: only the Q^{-2} decay remained. At large Q, the oscillation of the bilayer form factor was slightly shifted toward higher Q and the bilayer thickness was around 29 Å (Fig. SI5b). As for $R = 0.4$ in this region I.B, polydispersed spherical vesicles were observed by phase contrast microscopy at this temperature (Fig. 5b, right image and SI6f). Upon heating, the lamellar phases present in region II transit to large spherical vesicles that scatter light leading to turbid solution but without birefringence (Region I.B).

In regions III and IV, the two separated phases for $R = 0.6$ were characterized by SANS and the spectra are represented in Fig. 5c. In region III, three peaks were observed on the SANS spectrum of the upper phase, indicating the presence of lamellar phases in solution with a lamellar spacing of around 300 Å. Phase contrast microscopy experiments confirmed the presence of stacked lamellar phase in this upper birefringent phase (Fig. 5c, left image and SI7a and b). The SANS spectrum of the lower phase was completely different. At large Q, the spectrum can be fitted with a form factor of a sphere with a radius around 22 Å suggesting the formation of spherical micelles consistent with the limpidity of the samples. The scattered intensity decreased when going toward low-Q, demonstrating that the system has a low isothermal osmotic compressibility (Fig. SI5c). These micelles were composed of ionized fatty acids as shown by FT-IR and therefore bear negative charges at their surface. Then, micelles strongly repelled over large distances due to electrostatic repulsions, which gave rise to the broad correlation peak seen at around 0.032 $Å^{-1}$, which corresponds in the direct space to the average separation distance between micelles. Then, in region III, the upper part contained lamellar phases formed by the mixture of ionized and protonated fatty acid molecules as shown previously by FT-IR experiments and the lower part contained spherical micelles.

Upon heating, there was a transition from region III to region IV. The SANS spectra of the two phases in the region IV are represented in the Fig. 5c. Similarly as in region III, spherical micelles with a radius around 21 Å were present in the lower limpid phase (Fig. SI5c). For the upper phase, the SANS spectrum was similar to the one obtained for the upper phase in region III: three peaks were observed, typical from lamellar objects. However, vesicles have been observed by phase contrast microscopy in this part of the phase diagram (Fig. 5c, right image and Fig. SI7c). The self-assemblies in this upper phase were therefore multilamellar vesicles. Thus, upon heating, the lamellar phases present in region III corresponding to turbid solution with optical anisotropy transit into spherical multilamellar vesicles leading to non-birefringent turbid solution in region IV. Additional phase contrast microscopy images for the sample $R = 0.7$ are represented in Fig. SI7 in region III (d–e) and IV (f).

In region V, the samples were completely limpid. By phase contrast microscopy, no self-assembly of micron size was observed (Fig. 5d). The SANS spectra for $R = 1$ at 15 °C and 35 °C are represented in Fig. 5d. At large Q, the spectrum can be fitted with a form

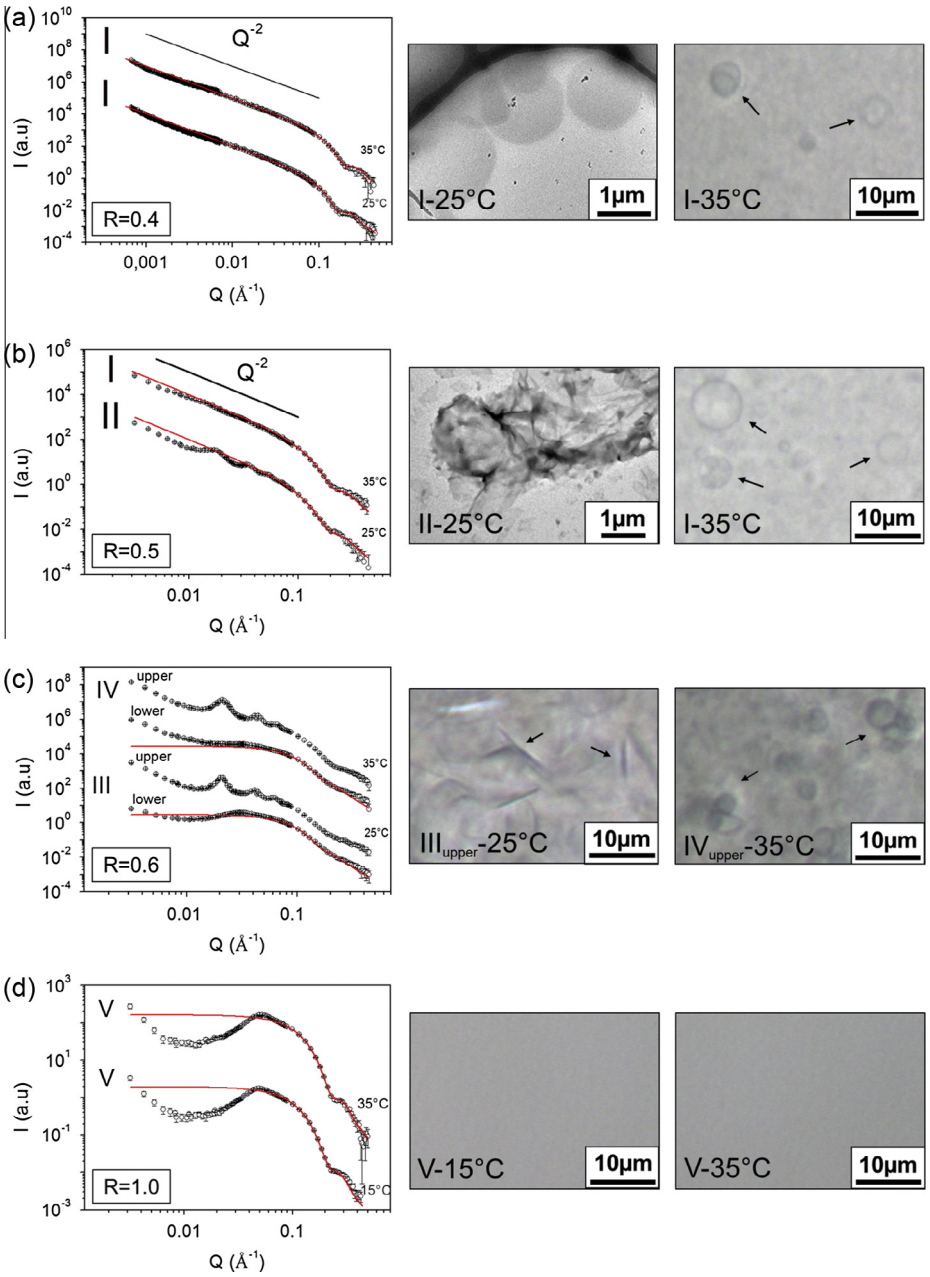

Fig. 5. SANS intensity profile for choline hydroxide/myristic acid solutions at different R and different temperatures with the corresponding microscopy images. The data were shifted in intensity for the sake of clarity. (a) SANS spectra for $R = 0.4$ in region I at 25 °C (bottom) and at 35 °C (top) with corresponding microscopy pictures. The facetted discs at low temperature was observed by cryo-TEM at 25 °C (left image) and spherical vesicles was observed by phase contrast microscopy at 35 °C (right image). (b) SANS profile for $R = 0.5$ in region II at 25 °C (bottom) and in region I at 35 °C (top) with the corresponding microscopy images of TEM for $R = 0.5$ in region II at 25 °C (left image) and phase contrast microscopy in region I at 35 °C (right image). (c) SANS profile for the upper and the lower phases for $R = 0.6$ at 25 °C in region III (bottom curves) and at 35 °C in region IV (top curves) with corresponding phase contrast microscopy pictures in region III at 25 °C (left image) and in region IV at 35 °C (right image). (d) SANS profile for $R = 1.0$ at 15 °C and 35 °C in the region V with corresponding phase contrast microscopy images at 15 °C (left image) and 35 °C (right image).

factor of a sphere with a radius of 18 Å (Fig. SI8). Additional SANS spectra in this region V are represented Fig. SI8 showing that spherical micelles with a radius of 18 Å were present for all $R > 1$.

3.4. Thermal behavior of fatty acid alkyl chains inside the bilayers self-assemblies

In the literature, it is known that the alkyl chains of the fatty acid embedded in bilayers self-assemblies may be either present in gel state ($L\beta$) or fluid state ($L\alpha$) as a function of temperature [11]. The transition between the two states is the so-called melting transition that is accompanied by a change in the thickness and fluidity of the bilayers. By SANS in region I and II, we showed that the bilayer thickness of the assemblies decreased with an increase of temperature, suggesting that such a phase transition occurred. To better understand this temperature effect, we coupled three additional techniques: Differential Scanning Calorimetry (DSC), solid state deuterium nuclear magnetic resonance (NMR) and Wide-Angle X-ray Scattering (WAXS) to investigate this system as a function of the temperature.

We first performed DSC measurements as a function of R (Fig. 6). For all R, a broad endothermic peak can be observed. The presence of this single endothermic peak is often associated with the melting transition of the surfactant chains [11]. For $R = 0.4$, a

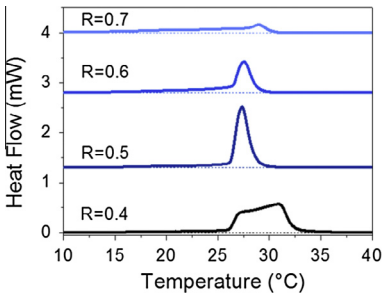

Fig. 6. Micro Differential Scanning Calorimetry endotherms obtained during heating scans for choline hydroxide/myristic acid solutions at different *R*. The spectra were shifted in intensity for clarity.

shoulder could be observed on the peak, probably due to the presence of a small amount of fatty acid crystals remaining in solution. The peak was slightly shifted to lower temperatures by increasing *R* and completely disappeared for $R > 0.8$ (Table SI1).

To check if the transition determined by DSC corresponds actually to the melting transition, NMR and WAXS experiments were performed. The NMR spectra for selected values of *R* are shown Fig. 7 (see also Fig. SI9). At 15 °C, below the transition detected by DSC, for the samples $R = 0.4$ (Region I) and $R = 0.5$ (Region II) a broad spectrum was observed, which is characteristic of fatty acids embedded in bilayers [30]. On these spectra, the larger quadrupolar splitting ($\Delta\upsilon \approx 56$ kHz) was attributed to the methylene groups in the alkyl chain and the lower at $\Delta\upsilon \approx 12$ kHz to the terminal –CD3 group. The isotropic peak ($\upsilon = 0$ kHz) stands for some remaining deuterated water. These values are characteristic of fatty acid embedded in a bilayer in the gel state ($L\beta$), with their alkyl chain in an all-trans conformation [11]. On WAXS spectra, a sharp peak was observed at 1.5 $Å^{-1}$ confirming that the alkyl chains were in a frozen state below the transition temperature determined by DSC (Fig. SI10) [11]. We can assess that the facetted discs and vesicles in region I and the lamellar phases in region II were made of fatty acid bilayers in gel state ($L\beta$).

Upon increasing the temperature above the phase transition determined by DSC ($T = 35$ °C), the NMR spectra were composed of doublets having splitting lower than those measured below the phase transition. The splitting were reduced ($\Delta\upsilon \approx 25$ kHz), which is characteristic of fatty acid embedded in the fluid bilayer state ($L\alpha$) [11]. At intermediate temperature, during the phase transition, NMR spectra were composed of a superimposition of the patterns observed below and above the transition temperature determined by DSC indicating the coexistence of bilayers in both the gel and fluid state. In the same way, the intensity of the sharp peak observed at 1.5 $Å^{-1}$ by WAXS decreased progressively with temperature until the end of the transition confirming the transition between the gel and the fluid state of the alkyl chains (Fig. SI10). Thus, in the region I at high temperature, spherical vesicles were made by fatty acid bilayers in fluid state ($L\alpha$). This melting of alkyl chains drives the transition from rigid objects such as facetted discs and vesicles (region I) or lamellar phases (regions II and III) to soft spherical vesicles (regions I and IV) with temperature.

4. Discussion

Our results are gathered in Scheme 1 that represents the self-assemblies observed in the choline hydroxide/myristic acid system as a function of *R* and temperature. It is known that the morphology of the self-assemblies is linked to the packing parameter defined as: $p = \frac{V}{a_0^c lc}$, where a_0 is the effective headgroup area and *V* is the volume of the hydrophobic chain possessing maximum effective length *lc* [6]. For $p < 1/3$, surfactant systems form spherical micelles. For $1/3 < p < 1/2$, worm-likes micelles are rather present. For $1/2 < p < 1$, bilayers or vesicles are obtained. In fatty acid systems, it is known that by tuning the ratio between ionized and protonated forms it is possible to change the self-assembled structure in solution due to a modification of a_0 [4,31].

The molar ratio between the choline hydroxide and the myristic acid drives the pH of the solution, which in turns control the ionization state of the fatty acids and the molecular interactions. Indeed, an increase of *R* leads to a pH increase due to the addition of hydroxide ions with the choline cation. For $R > 1$ corresponding to high pH value, we showed that all myristic acid molecules were under their ionized form. Choline is known to be bound only weakly to the fatty acid carboxylate group [25]. Choline is a weakly hydrated ion acting as a chaotrope and can promote fatty acid

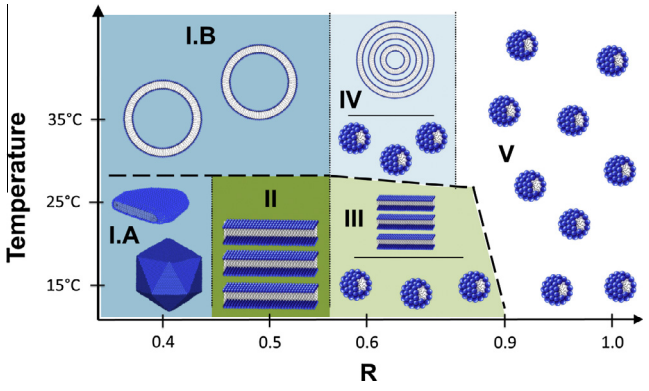

Scheme 1. Schematic representation of the phase behavior of the choline hydroxide/myristic acid system as a function of both molar ratio *R* and temperature.

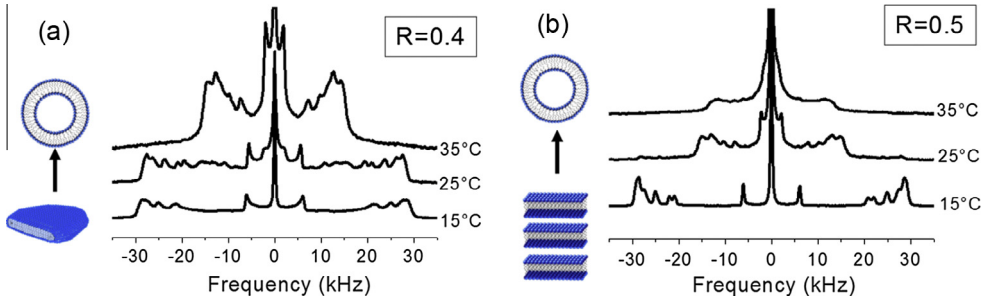

Fig. 7. Deuterium NMR spectra of the choline hydroxide/myristic acid system at (a) $R = 0.4$ and (b) $R = 0.5$, at three temperatures 15 °C, 25 °C and 35 °C. The spectra were shifted in intensity for clarity. In the phase diagram, the samples $R = 0.4$ and $R = 0.5$ transit in the region I from facetted objects to spherical vesicles and from lamellar phases to spherical vesicles with temperature, respectively.

self-assemblies of high curvature such as micelles [25]. In these conditions, the headgroup area is large and the repulsive interactions between ionized headgroups induce an important radius of curvature of the aggregate. The packing parameter should be inferior to 1/3 and spherical micelles were formed in solution leading to limpid solution (region V).

By decreasing R, we showed that the pH decreased and that the two states of fatty acid molecules (ionized and protonated forms) coexist. Hydrogen bonds can thus be formed between both the two types of forms. It is known that hydrogen bonding causes a decrease of the a_0 value and then a concomitant increase of the packing parameter, which is favorable for the formation of planar structures [33,34]. In solution, we highlighted the presence of lamellar phases (region II), facetted discs and vesicles (region I), which is in agreement with the self-assembly shape predicted by the packing parameter concept. We suppose that facetted objects are obtained for $R = 0.4$ in Region I due to a segregation process, which is well-known to occur in catanionic systems based on myristic acid [14,15]. In such segregation process, we suppose that one part of ionized fatty acids are expulsed to form the edges of the faceted vesicles or the micron-size discs and that the faces of these objects are mainly composed of protonated fatty acids forming a rigid bilayer with alkyl chains in gel state [18,35–37]. It is likely that the fine tuning of R in the range $0.35 < R < 0.45$, which in turn modifies the amount of ionized fatty acids, can control the size and the quantity of each facetted objects as shown in catanionic systems based on myristic acid and CTAOH [14,15].

In the intermediate range of R (regions III and IV), a slow macroscopic phase separation occurred with time: the upper phase was composed by lamellar phases (region III) or spherical vesicles (region IV) and the lower phase was composed by spherical micelles. The two self-assemblies coexisted as a function of the temperature until the creaming process occurred with time. The aggregation number between spherical micelles, lamellar phases or vesicles being very different from one morphology to another, the local fatty acid concentration in solution is very different in the different phases. Since the density of fatty acid molecules is lower than water, the density of the phase containing lamellar phases or vesicles is lower than the density of the phase containing spherical micelles. This difference of density leads to the progressive creaming of the lamellar phases or vesicles with time toward the upper part of the vial and ultimately to the macroscopic phase separation [17].

We observed that the temperature is another parameter which can be used to trigger the self-assembly transitions in this system. At low R, facetted objects or lamellar phases transform into spherical vesicles with temperature. We highlighted that temperature affected the self-assembly structure because of the chain melting process. During this melting process, the aliphatic chains changed from a rigid and ordered gel state to a fluid state in which bilayers become more flexible and the molecules gained a disordered state leading to more flexible self-assemblies with higher curvature. The transition between the facetted objects or lamellar phases to spherical vesicles is reversible due to the reversibility of the melting phenomenon. This behavior with temperature has already been observed for similar fatty acid catanionic systems [4,11,38].

Conclusion

In this study, we investigated the impact of the molar ratio R and temperature on the phase behavior of myristic acid and choline hydroxide system. As for salt-free catanionic systems based on fatty acid and cationic surfactant in its hydroxide form, various self-assemblies have been obtained by tuning R: facetted objects (vesicles coexisting with discs), lamellar phases, and spherical micelles. An increase of R induces a rise of pH and consequently, a change in the ionization state of the myristic acid. The ratio between the two forms of the fatty acid (ionized and protonated), can be finely tuned by R, which in turn regulates the molecular interactions (hydrogen bonding and electrostatic interactions) and accordingly the resulting packing parameter. We showed that temperature can induce self-assembly transitions in solution. The chain melting process of the fatty acid chains, which modifies the bilayer state inside the aggregates from gel rigid state to fluid state, leads to the transition from facetted objects (vesicles and discs) or lamellar phases to spherical vesicles. A broad polymorphism can be easily obtained in this system by tuning both R and temperature.

Our study provides a deep understanding of the processes at play in fatty acids/quaternary ammonium counter-ion systems, which should be helpful not only for a better understanding of fatty acid system in the presence of quaternary ammonium counter-ion, but also for further broadening the potential applications of fatty acid choline soaps as green surfactants since they are considered to be highly biocompatible and environmentally safe [22,23].

Acknowledgment

A. Arnould would like to thank the region Pays de la Loire and l'INRA for the allocation of her PhD grant. We acknowledge the experimental assistance of B. Houinsou-Houssou. We thank Laboratoire Léon Brillouin for the beam time allocation on the spectrometer PACE and TPA and Dr. A. Brûlet for her help during the neutron scattering run. Access to the NMR facilities on the BIBS platform (Biopolymères Interactions Biologie Structurale) of INRA Angers-Nantes was greatly appreciated and we would like to thank L. Foucat and X. Falourd for their help during these experiments. We thank also B. Pontoire for his help during the WAXS measurements and Dr. B. Bakan for her help during the FT-IR experiments. We gratefully acknowledge Dr. A. Salonen, Dr. A. Saint-Jalmes and Dr. J. Ravaux for the useful discussions.

Appendix A. Supplementary material

Supplementary data associated with this article can be found, in the online version, at http://dx.doi.org/10.1016/j.jcis.2015.01.008.

References

[1] I. Johansson, M. Svensson, Curr. Opin. Colloid Interface Sci. 6 (2001) 178–188, http://dx.doi.org/10.1016/S1359-0294(01)00076-0.
[2] A.-L. Fameau, C. Gaillard, D. Marion, B. Bakan, Green Chem. 15 (2013) 341–346, http://dx.doi.org/10.1039/c2gc36677k.
[3] M. Svensson, Surfactants based on natural fatty acids, in: M. Kjellin, I. Johansson (Eds.), Surfactant from Renew. Resour., John Wiley & Sons Ltd., 2010, pp. 1–19, http://dx.doi.org/10.1002/9780470686607.
[4] A.-L. Fameau, A. Arnould, A. Saint-Jalmes, Curr. Opin. Colloid Interface Sci. 19 (2014) 471–479, http://dx.doi.org/10.1016/j.cocis.2014.08.005.
[5] J.W. McBain, J. Am. Chem. Soc. 50 (1928) 1636–1640, http://dx.doi.org/10.1021/ja01393a016.
[6] J.N. Israelachvili, Intermolecular and Surface Forces, third ed., Elsevier, London, 2010.
[7] C. Madelmont, K. Perron, Colloid Polym. Sci. 254 (1976) 581–595, http://dx.doi.org/10.1007/BF01382576.
[8] A.-L. Fameau, S. Lam, O.D. Velev, Chem. Sci. 4 (2013) 3874–3881, http://dx.doi.org/10.1039/c3sc51774h.
[9] A.-L. Fameau, A. Saint-Jalmes, F. Cousin, B. Houinsou Houssou, B. Novales, L. Navailles, et al., Angew. Chem. 123 (2011) 8414–8419, http://dx.doi.org/10.1002/ange.201102115.
[10] D. Varade, D. Carriere, L.R. Arriaga, A.-L. Fameau, E. Rio, D. Langevin, et al., Soft Matter 7 (2011) 6557–6570, http://dx.doi.org/10.1039/c1sm05374d.
[11] A.-L. Fameau, T. Zemb, Adv. Colloid Interface Sci. 207 (2014) 43–64, http://dx.doi.org/10.1016/j.cis.2013.11.017.
[12] J.M. Gebicki, M. Hicks, Nature 243 (1973) 232–234, http://dx.doi.org/10.1038/243232a0.

[13] J. Hao, H. Hoffmann, Curr. Opin. Colloid Interface Sci. 9 (2004) 279–293, http://dx.doi.org/10.1016/j.cocis.2004.06.004.
[14] M. Dubois, B. Demé, T. Gulik-Krzywicki, Jean-C. Dedieu, C. Vautrin, S. Désert, et al., Nature 411 (2001) 672–675, http://dx.doi.org/10.1038/35079541.
[15] T. Zemb, M. Dubois, B. Démé, T. Gulik-Krzywicki, Science 283 (1999) 816–819, http://dx.doi.org/10.1126/science.283.5403.816 (80-).
[16] A. Song, S. Dong, X. Jia, J. Hao, W. Liu, T. Liu, Angew. Chem. Int. Ed. Engl. 44 (2005) 4018–4021, http://dx.doi.org/10.1002/anie.200500353.
[17] H. Li, J. Hao, J. Phys. Chem. B 112 (2008) 10497–10508, http://dx.doi.org/10.1021/jp802235g.
[18] M. Dubois, V. Lizunov, A. Meister, T. Gulik-Krzywicki, J.M. Verbavatz, E. Perez, et al., Proc. Natl. Acad. Sci. U. S. A. 101 (2004) 15082–15087, http://dx.doi.org/10.1073/pnas.0400837101.
[19] R. Zana, Langmuir 20 (2004) 5666–5668, http://dx.doi.org/10.1021/la040033i.
[20] R. Klein, D. Touraud, W. Kunz, Green Chem. 10 (2008) 433–435, http://dx.doi.org/10.1039/b718466b.
[21] G. Li, Y. Liu, W. Xu, J. Hao, A. Song, J. Phys. Chem. B (2014), http://dx.doi.org/10.1021/jp510747y.
[22] R. Klein, E. Müller, B. Kraus, G. Brunner, B. Estrine, D. Touraud, et al., RSC Adv. 3 (2013) 23347–23354, http://dx.doi.org/10.1039/c3ra42812e.
[23] D. Rengstl, B. Kraus, M. Van Vorst, G.D. Elliott, W. Kunz, Colloids Surf. B Biointerfaces 123 (2014) 575–581, http://dx.doi.org/10.1016/j.colsurfb.2014.09.057.
[24] Y. Han, Z. Chu, H. Sun, Z. Li, Y. Feng, RSC Adv. 2 (2012) 3396–3402, http://dx.doi.org/10.1039/c2ra20136d.
[25] R. Klein, M. Kellermeier, M. Drechsler, D. Touraud, W. Kunz, Colloids Surf. A Physicochem. Eng. Asp. 338 (2009) 129–134, http://dx.doi.org/10.1016/j.colsurfa.2008.04.049.
[26] R. Klein, G.J.T. Tiddy, E. Maurer, D. Touraud, J. Esquena, O. Tache, et al., Soft Matter 7 (2011) 6973–6983, http://dx.doi.org/10.1039/c1sm05108c.
[27] D. Rengstl, O. Diat, R. Klein, W. Kunz, Langmuir 29 (2013) 2506–2519, http://dx.doi.org/10.1021/la304431c.
[28] A. Brûlet, D. Lairez, A. Lapp, J.-P. Cotton, J. Appl. Crystallogr. 40 (2007) 165–177, http://dx.doi.org/10.1107/S0021889806051442.
[29] A. Brûlet, V. Thévenot, D. Lairez, S. Lecommandoux, W. Agut, S.P. Armes, et al., J. Appl. Crystallogr. 41 (2008) 161–166, http://dx.doi.org/10.1107/S0021889807056361.
[30] J.H. Davis, Biochim. Biophys. Acta – Rev. Biomembr. 737 (1983) 117–171, http://dx.doi.org/10.1016/0304-4157(83)90015-1.
[31] K. Morigaki, P. Walde, Curr. Opin. Colloid Interface Sci. 12 (2007) 75–80, http://dx.doi.org/10.1016/j.cocis.2007.05.005.
[32] S. Song, Q. Zheng, A. Song, J. Hao, Langmuir 28 (2012) 219–226, http://dx.doi.org/10.1021/la203581m.
[33] W. Xu, X. Wang, Z. Zhong, A. Song, J. Hao, J. Phys. Chem. B 117 (2013) 242–251, http://dx.doi.org/10.1021/jp306630n.
[34] W. Xu, A. Song, S. Dong, J. Chen, J. Hao, Langmuir 29 (2013) 12380–12388, http://dx.doi.org/10.1021/la403008d.
[35] J. Hao, W. Liu, G. Xu, L. Zheng, Langmuir 19 (2003) 10635–10640, http://dx.doi.org/10.1021/la030065q.
[36] M.A. Greenfield, L.C. Palmer, G. Vernizzi, M.O. de la Cruz, S.I. Stupp, J. Am. Chem. Soc. 131 (2009) 12030–12031, http://dx.doi.org/10.1021/ja903546y.
[37] Y. Shen, Z. Ou-Yang, Y. Zhang, J. Hao, Z. Liu, Langmuir 30 (2014) 2632–2638, http://dx.doi.org/10.1021/la403279c.
[38] Y. Shen, J. Hao, H. Hoffmann, Z. Wu, Soft Matter 4 (2008) 805–810, http://dx.doi.org/10.1039/b717097a.